Journal of Advanced Ceramics
2016, **5**(1): 77–83
DOI: 10.1007/s40145-015-0175-8

ISSN 2226-4108
CN 10-1154/TQ

Research Article

Nanocrystalline $BaTi_2O_5$ dielectric ceramic prepared by full crystallization from containerless solidified glass

Jianqiang LI[a], Guoqing BA[a], Xiwei QI[b], Xiaoyu LI[a,*], Yingcui SONG[a,c], Bo LI[c]

[a]*National Engineering Laboratory for Hydrometallurgical Cleaner Production Technology*, *Key Laboratory of Green Process and Engineering*, *Institute of Process Engineering*, *Chinese Academy of Sciences*, *Beijing 100190*, *China*
[b]*School of Resources and Materials*, *Northeastern University at Qinhuangdao*, *Qinhuangdao 066004*, *China*
[c]*Research Institute for Advanced Materials*, *Graduate School at Shenzhen*, *Tsinghua University*, *Shenzhen 518055*, *China*

Received: August 25, 2015; Revised: October 28, 2015; Accepted: November 11, 2015

Abstract: We show that fully dense nanocrystalline titanate ceramic could be obtained by full crystallization from glass which was prepared by a novel contactless solidification process. Through annealing above glass transition temperature T_g for prescribed duration, $BaTi_2O_5$ ceramic with grain size of 20–130 nm was successfully fabricated. The dependence of the nanoceramic's dielectric constant and dissipation on frequency was investigated. The results show clearly that the dielectric constant of $BaTi_2O_5$ nanoceramic depends on average grain size in nanometer scale, and an optimal range of the grain size is found which exhibits greater dielectric constant than conventional microcrystalline ceramics. The as-fabricated ceramic also possesses lower dielectric dissipation, which can be mainly attributed to the presence of nanometer-sized grains.

Keywords: nanocrystalline ceramic; glass; $BaTi_2O_5$; containerless solidification; dielectric properties

1 Introduction

Nanocrystalline ceramics are a promising class of novel materials for a diverse range of applications in electronics, mechanics, and optics, etc. [1–6]. A number of nanocrystalline ceramics have been fabricated by using spark plasma sintering (SPS) [7,8], two-step sintering [9,10], microwave sintering [11], ultra-high pressure sintering [12], and so on [13,14]. SPS is used as a good method of preparing ceramics with pure phase because of short duration within sintering process [15]. Two-step sintering has a short high temperature sintering followed by a long low temperature treatment to frozen the grain boundary migration, which can obtain nanocrystalline ceramics [10]. Microwave and ultra-high pressure sintering are recognized as two effective routes to fabricate ceramics by sintering the nanopowder [11,12]. Despite these achievements, obstacles remain on the path forward to widespread deployment of dense nanocrystalline ceramics. Current solid-state synthetic approaches are expensive, requiring nanometer-sized raw materials and demanding to elaborately design sintering temperature and duration. In principle, an approach, in which dense and chemically homogenous polycrystalline materials are obtained by direct

* Corresponding author.
E-mail: lixy@ipe.ac.cn

crystallization from glass, would have many of these obstacles. There has been considerable work on transparent glass–ceramic systems, which consist of microcrystalline and glassy phases [16–18]. However, to the best of our knowledge, there are few reports of nanocrystalline ceramics attained by a complete, direct bulk glass crystallization synthesis route.

$BaTi_2O_5$ has been discovered as a new ferroelectric compound by Akashi *et al.* [19,20] and Akishige *et al.* [21]. The single-crystalline $BaTi_2O_5$ prepared by floating zone melting shows a high Curie temperature (T_C = 430–475 ℃) and a high permittivity in *b*-direction without lead additives [19,20]. Hence, $BaTi_2O_5$ ceramic is fabricated and studied as a promising environmentally friendly material [15,21–24]. Polycrystalline $BaTi_2O_5$ ceramic was prepared by laser rapid solidification method [22]. Highly dense $BaTi_2O_5$ ceramic was effectively fabricated by spark plasma sintering method [15]. Another synthetic approach for single-phase $BaTi_2O_5$ ceramic is hot-pressing the arc-melting-derived needle-like powder [23]. However, since $BaTi_2O_5$ can be easily decomposed into $BaTiO_3$ and $Ba_6Ti_{17}O_{40}$ above 1500 K, bulk $BaTi_2O_5$ ceramic can still be hardly prepared by using conventional solid-state sintering approach [25–27].

Recently, Yu and coworkers [28,29] fabricated $BaTi_2O_5$ glass in ~2 mm ellipsoidal bulk form without adding any network-forming oxides. Their method involved a containerless solidification process by using an aerodynamic levitator (ADL), which enables molten materials deep undercooling because it suppresses inhomogeneous nucleation from the container wall. The structural analysis revealed that the $BaTi_2O_5$ glass obtained by this way has unusual features, consisting of distorted Ti–O polyhedra with an average coordination number of approximately 5 [30,31]. As a result, $BaTi_2O_5$ glass possesses very high refractive index exceeding 2.1 and an anomalous permittivity (more than 10^7) near glass transition temperature T_g [28,31]. Till today, there is no report of fully dense nanocrystalline $BaTi_2O_5$ ceramic directly fabricated by bulk glass crystallization synthesis route, neither report on the relationship between dielectric properties of nanostructured $BaTi_2O_5$ ceramic and grain size.

In this work, nanocrystalline single-phase $BaTi_2O_5$ ceramic was directly obtained by crystallization from a containerless solidified glassy precursor. The dielectric properties of nanocrystalline ceramic with different annealing treatment depended on frequency were investigated, and it was found that the dielectric constant of $BaTi_2O_5$ nanoceramic depends on average grain size in nanometer scale, and there is an optimal range of grain size which exhibits greater dielectric constant than conventional microcrystalline ceramics. Moreover, the dielectric dissipation of as-fabricated ceramic is also lower than that of microcrystalline ceramics. The reason could be mainly attributed to the presence of nanometer-sized grains.

2 Experimental

The glass precursor was synthesized employing an aerodynamic levitator furnace equipped with CO_2 laser allowing for the high temperature melt and rapid quenching under noncontact process by shutting down the laser. Firstly, to prepare samples for levitation, high purity (99.9%) $BaTiO_3$ and TiO_2 were fully mixed at a 1:1 molar ratio, pressed into pellets, sintered for the first time at 1400 K for 8 h and then at 1420 K for 12 h for the second time. Cylinder samples of 35 mg made from the pellets were put into the furnace and levitated by O_2 flow. After heating the samples up to 2100 K, glassy transparent spheres with diameter of about 2.5 mm were obtained from deep undercooled melt through a containerless solidification process. The glassy spheres were then crystallized into nanocrystalline ceramic in a highly accurate annealing furnace (KSL-1100X, Hefei Kejing Materials Technology Co. Ltd.) at a series of temperatures ranging from 960 to 1020 K and duration ranging from 10 to 60 min in order to find out the effects of these factors on dynamic crystallization process.

The crystallization temperature in synthesis of nanocrystalline $BaTi_2O_5$ ceramic was determined by differential scanning calorimetry (DSC, Netzsch STA 449 F3 Jupiter) measurement. Phase characterization was performed on X-ray diffraction (XRD, Philips X'Pert Pro MPD, Philips), and structure determination of the annealed samples etched by HF aqueous solution for 80 s was performed using a scanning electron microscope (SEM, JSM-6700F, JEOL). Dielectric characterizations were determined by a dielectric analysis system (HP 4294A, Agilent Inc.).

3 Results and discussion

3.1 Determination of the annealing temperature

The as-solidified $BaTi_2O_5$ samples are ~2 mm

transparent spheres without any pore. The glassy feature of the samples was confirmed by XRD given in Fig. 1, which shows the samples are highly amorphous except for a small trace of crystalline $BaTi_2O_5$ whose peak corresponds to the most intense reflection of $BaTi_2O_5$.

In order to determine the proper annealing temperature for the $BaTi_2O_5$ glass crystallization, DSC measurement was employed to investigate the phase transition process. Figure 2 shows that the glass transition temperature (T_g) and crystallization temperatures ($T_{\alpha x}$ and $T_{\beta x}$) are clearly presented at exothermic peaks, and T_g, $T_{\alpha x}$, and $T_{\beta x}$ are 973, 993, and 1020 K, respectively. Yu *et al.* [32] found a giant dielectric constant 10^7 at the first exothermic peak during continuous temperature rise, then dropping rapidly to 10^6 within the following 20 K. With reference to above results, we made a configuration including the annealing temperature and duration (samples with different annealing temperature for duration 10 min are numbered as S_i; samples with different duration at annealing temperature 1000 K are numbered as s_i) as listed in Table 1.

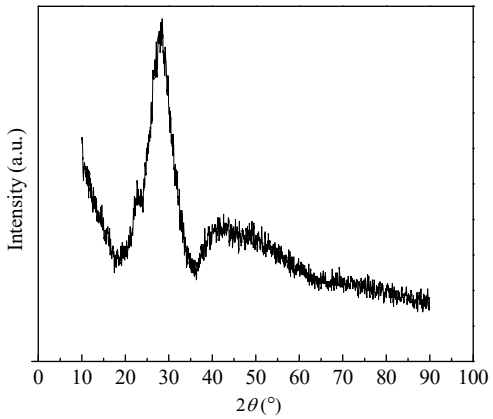

Fig. 1 XRD pattern of $BaTi_2O_5$ glass.

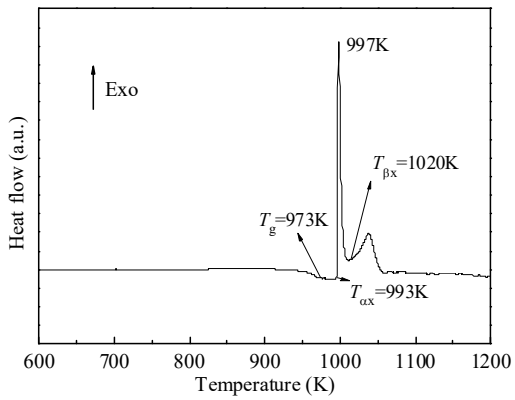

Fig. 2 DSC curve of $BaTi_2O_5$ glass.

Table 1 Annealing parameter of $BaTi_2O_5$ glass

Sample	Temperature (K)	Duration (min)	Sample	Temperature (K)	Duration (min)
S_1	960	10	s_1	1000	10
S_2	980	10	s_2	1000	20
S_3	1000	10	s_3	1000	40
S_4	1020	10	s_4	1000	60

By simple observation with naked eyes, transparency of the annealed $BaTi_2O_5$ glass decreases as the treating temperature increases and treating duration rises. S_4, s_3, and s_4 are milk white and opaque. It is supposed that the decrease in transparency is related with crystallization of the glass because its thermodynamics and kinetics instabilities increase with increase of both annealing temperature (higher than T_g and $T_{\alpha x}$) and duration [33].

3.2 Phase composition of nanometer-sized $BaTi_2O_5$ ceramic

Figure 3 gives the XRD patterns of the annealed $BaTi_2O_5$ glass from 960 to 1020 K for the same duration (10 min). Typical amorphous broad peak of $BaTi_2O_5$ glass disappears and some characterized Bragg peaks of $BaTi_2O_5$ ceramic emerge at 960 K. This phenomenon perfectly matches with our DSC results that the glass begins to crystallize at 960 K (T_g = 973 K). As the annealing temperature increases from 980 to 1020 K for the same annealing duration, sharp crystallized peaks constantly emerge, suggesting higher crystallization.

Figure 4 shows the XRD patterns of annealed glass at 1000 K for varied duration from 10 to 60 min. It can be concluded that sample crystallinity increases as the annealing duration rises, Bragg peaks are almost characterized $BaTi_2O_5$ peaks, and peaks of $Ba_6Ti_{17}O_{40}$ disappear after 40 min annealing treatment at 1000 K.

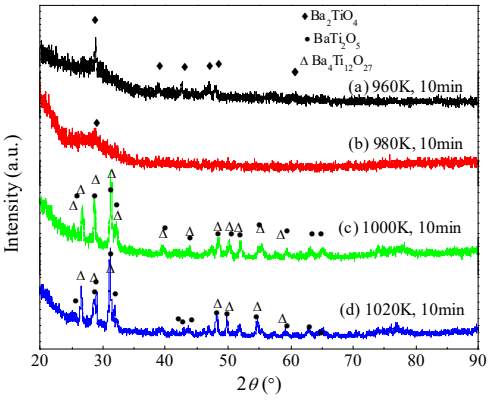

Fig. 3 XRD patterns of varied $BaTi_2O_5$ glass annealed at (a) 960 K, (b) 980 K, (c) 1000 K, (d) 1020 K for 10 min.

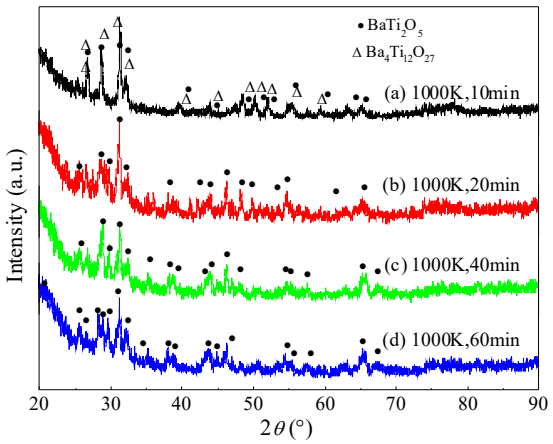

Fig. 4 XRD patterns of varied $BaTi_2O_5$ glass annealed at 1000 K for (a) 10 min, (b) 20 min, (c) 40 min, (d) 60 min.

For the sample after 60 min annealing treatment at 1000 K, the XRD pattern shows pure $BaTi_2O_5$ crystalline phase.

3. 3 Microstructure of $BaTi_2O_5$

Surface morphology of HF etched $BaTi_2O_5$ glass reveals a typical amorphous appearance without grain boundary. Microstructures represented in Figs. 5(a) and 5(b) are similar with that of $BaTi_2O_5$ glass except for a few gully shape structures in accordance with $BaTi_2O_5$ emergence in Fig. 3. Several spherical structures are observed on amorphous matrix shown in Fig. 5(c) and these areas may be $BaTi_2O_5$ and $Ba_4Ti_{12}O_{27}$ by referring to XRD patterns in Fig. 3. A mass of spherical and hemispherical structures appear in Fig. 5(d) and the average grain size is 50–150 nm. Observed in Fig. 2, 1020 K is the transition temperature of α-phase to β-phase, so the principal crystalline phase is $BaTi_2O_5$ after 10 min treatment at 1020 K. In Fig. 6, as the increase of annealing duration

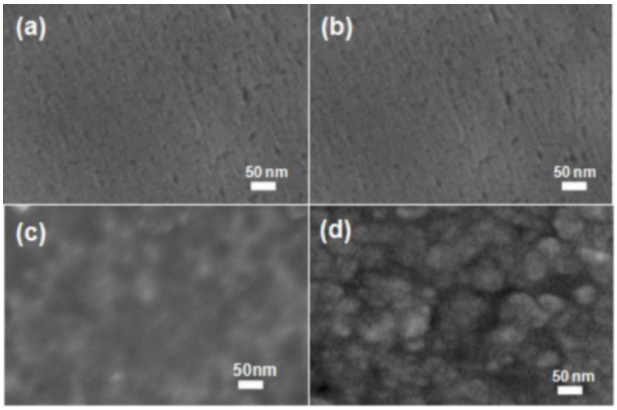

Fig. 5 SEM micrographs of varied $BaTi_2O_5$ glass after different annealing temperature at (a) 960 K, (b) 980 K, (c) 1000 K, (d) 1020 K for 10 min.

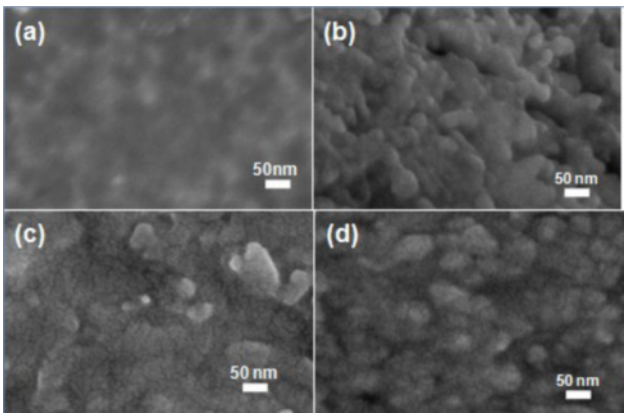

Fig. 6 SEM micrographs of varied $BaTi_2O_5$ glass after different annealing duration at 1000 K for (a) 10 min, (b) 20 min, (c) 40 min, (d) 60 min.

at 1000 K, grain crystallizes into regular shape and grows. The sample has been totally crystallized into $BaTi_2O_5$ phase with spherical and elliptical grains of 50–150 nm in Fig. 6(d). Materials that reveal pore-free, fully dense polycrystalline with nanostructures are shown in Figs. 5 and 6.

Table 2 shows the average grain size of $BaTi_2O_5$ glass under different annealing process. The annealed $BaTi_2O_5$ glass samples from 960 to 1000 K for 10 min (S_1 and S_2) do not have obvious crystallization. Average grain sizes of samples increase with increase of annealing temperature and duration. These results are well agreeable with that from XRD patterns.

3. 4 Dielectric properties

In this work, the frequency dependence of permittivity was measured with an impedance analyzer. For initial measurement, our annealed samples were cut into disks of 0.4 mm in thickness and 2.44 mm in diameter, and Ag was coated as electrode. Figure 7 shows the frequency dependence of permittivity (ε_r) and loss component ($\tan\delta$) of annealed $BaTi_2O_5$ glass. When the annealing temperature is below 1000 K, permittivity of the annealed glass is similar with untreated glass with the increase of temperature after the same processing duration. When it comes to 1020 K, there is a jump of permittivity which indicates a change in crystal structure introduced by annealing treatment. The above phenomenon is in good agreement with our XRD

Table 2 Average grain size of $BaTi_2O_5$ annealed at different process

Sample	S_1	S_2	S_3	S_4	s_1	s_2	s_3	s_4
Average grain size (nm)	—	—	20	50	20	50	80	130

patterns and SEM micrographs: crystallization occurs in our sample only when it reaches 1000 K, and Bragg peaks begin to grow in both number and amplitude at 1020 K. The average grain size is more than 50 nm, which is bigger than that under 1000 K annealing temperature. All of those changes in both structure and grain size lead to the jump of permittivity at 1020 K.

As shown in Fig. 7(b), when samples are annealed under 1000 K, tanδ of different samples stay the same with the increase of annealing temperature; however, there is a decrease of tanδ of the same sample with frequency increasing. When the sample is annealed above 1020 K, tanδ increases with temperature and frequency which is different with tendency of other curves below 1000 K. That may be attributed to the presence of β-phase crystalline $BaTi_2O_5$ after 10 min treatment at 1020 K, as DSC curve indicates that 1020 K is the transition temperature of α-phase to β-phase [32].

In Fig. 8(a), the dielectric constant increases with duration increasing from 10 to 40 min and decreases with frequency increasing for ceramic annealed under 1000 K; however, it decreases with the grain size growth when the nanoceramic is annealed at 1000 K for 60 min, which indicates an optimal grain size contributes to the greatest dielectric constant. tanδ decreases with frequency increasing for ceramic annealed under 1000 K, 10 min treatment, but it increases with frequency and annealing duration increasing subsequently, which is corresponded with SEM micrographs: as the grain grows, tanδ increases.

The result shows there is strong dependence of dielectric properties such as ε_r and tanδ on average grain size of nanoceramic. When grain size is below 100 nm, remarkable surface effect, volume effect, and quantum size effect lead to notable changes in optical, thermal, and electromagnetic performances for the samples.

Value of tanδ for $BaTi_2O_5$ nanocrystalline ceramic shown in Fig. 8(b) is lower than the value of which was fabricated by other methods. The decrease of tanδ is a consequence of the following mechanism. As the grain size gets smaller, nanometer-sized grain becomes active and degree of spontaneous polarization decreases, thus under the function of electric field, lower energy is required for dipoles to change directions.

Polarization of a dielectric material is the sum of the contributions of electronic, dipolar, ionic, and interfacial polarizations [34]. At low frequency, all the

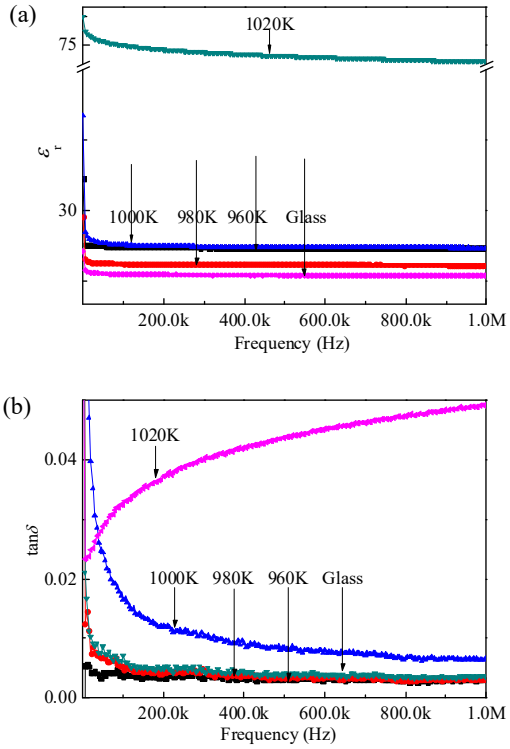

Fig. 7 Frequency dependence of (a) dielectric constant ε_r and (b) tanδ of $BaTi_2O_5$ ceramic annealed at different temperatures for 10 min.

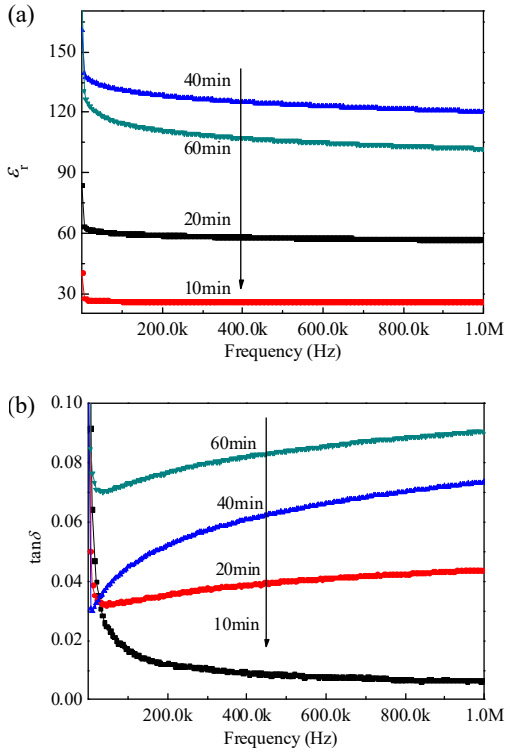

Fig. 8 Frequency dependence of (a) dielectric constant ε_r and (b) tanδ of $BaTi_2O_5$ ceramic annealed at 1000 K for different duration.

polarizations occur in varying electric field, but at higher frequency, a main contributor of ε_r is electronic polarization, since some of the polarizations become ineffective, as a result, the net polarization mobility of the material decreases which leads to the decrease in the value of ε_r [35]. The increase in loss tangent, observed at room temperature as a function of frequency, can be ascribed to the mobility enhancement of the ionic charge carriers.

4 Conclusions

In conclusion, by varying the annealing temperature and duration, nanocrystalline ceramic was successfully fabricated by containerless solidification following quick annealing, and its dielectric properties are in obvious difference with traditional materials in many aspects. Compared with permittivity value (around 70) of $BaTi_2O_5$ with micrometer grain size, ε_r of $BaTi_2O_5$ nanocrystalline ceramic with 80 nm average grain size reaches the highest value of above 130 (room temperature, 100 kHz). So there is an optimal range of grain size for nanocrystalline ceramic exhibiting better permittivity properties than microcrystalline ceramics due to quantum size effect. It is anticipated that the economical and innovative preparation approach presented here can be widely applied to fabricate other dense, chemically homogenous polycrystalline nanometer materials.

Acknowledgements

This work was financially supported by the National Natural Science Foundation of China (Grant Nos. 51471158, 51274182, and 51474061) and Beijing Natural Science Foundation (Nos. 2152032 and 2112039).

References

[1] Andrievski RA, Glezer AM. Size effects in properties of nanomaterials. *Scripta Mater* 2001, **44**: 1621–1624.
[2] Parashar SKS, Choudhary RNP, Murty BS. Electrical properties of Gd-doped PZT nanoceramic synthesized by high-energy ball milling. *Mat Sci Eng B* 2004, **110**: 58–63.
[3] Mukhopadhyay A, Basu B. Consolidation–microstructure–property relationships in bulk nanoceramics and ceramic nanocomposites: A review. *Int Mater Rev* 2007, **52**: 257–288.
[4] Madtha S, Ravi Chandran KS. Reactive-sinter-processing and attractive mechanical properties of bulk and nanostructured titanium boride. *J Am Ceram Soc* 2012, **95**: 117–125.
[5] Zaleski AJ, Nyk M, Strek W. Magnetic studies of GaN nanoceramics. *Appl Phys Lett* 2007, **90**: 042511.
[6] Gizhevskii BA, Sukhorukov YP, Loshkareva NN, *et al.* Optical absorption spectra of nanocrystalline cupric oxide: Possible effects of nanoscopic phase separation. *J Phys: Condens Matter* 2005, **17**: 499–506.
[7] Nishimura T, Mitomo M, Hirotsuru H, *et al.* Fabrication of silicon nitride nano-ceramics by spark plasma sintering. *J Mater Sci Lett* 1995, **14**: 1046–1047.
[8] Song S-H, Zhu Q-S, Weng L-Q, *et al.* A comparative study of dielectric, ferroelectric and magnetic properties of $BiFeO_3$ multiferroic ceramics synthesized by conventional and spark plasma sintering techniques. *J Eur Ceram Soc* 2015, **35**: 131–138.
[9] Chen I-W, Wang X-H. Sintering dense nanocrystalline ceramics without final-stage grain growth. *Nature* 2000, **404**: 168–171.
[10] Zhou C, Xie P, Chen Y, *et al*. Synthesis, sintering and characterization of porous nano-structured CaP bioceramics prepared by a two-step sintering method. *Ceram Int* 2015, **41**: 4696–4705.
[11] Demirskyi D, Agrawal D, Ragulya A. Tough ceramics by microwave sintering of nanocrystalline titanium diboride ceramics. *Ceram Int* 2014, **40**: 1303–1310.
[12] Lu TC, Chang XH, Qi JQ, *et al.* Low-temperature high-pressure preparation of transparent nanocrystalline $MgAl_2O_4$ ceramics. *Appl Phys Lett* 2006, **88**: 213120.
[13] Hirano M, Minagawa K. Solid solution nanocrystals in the CeO_2–Y_3NbO_7 system: Hydrothermal formation and control of crystallite growth of ceria. *J Am Ceram Soc* 2014, **97**: 3800–3806.
[14] Dey S, Drazin JW, Wang Y, *et al.* Radiation tolerance of nanocrystalline ceramics: Insights from yttria stabilized zirconia. *Sci Rep* 2015, **5**: 7746.
[15] Liu W, Tsukada S, Li S, *et al.* Effect of spark plasma sintering temperature on the phase equilibria and dielectric properties of $BaTi_2O_5$ ceramics. *J Mater Sci* 2014, **49**: 7908–7914.
[16] Wan W, Liu C, Sun H, *et al.* Low-toxic gelcasting of giant dielectric-constant $CaCu_3Ti_4O_{12}$ ceramics from the molten salt powder. *J Eur Ceram Soc* 2015, **35**: 3529–3534.
[17] Beall GH, Pinckney LR. Nanophase glass-ceramics. *J Am Ceram Soc* 1999, **82**: 5–16.
[18] Allix M, Alahrache S, Fayon F, *et al.* Highly transparent $BaAl_4O_7$ polycrystalline ceramic obtained by full crystallization from glass. *Adv Mater* 2012, **24**: 5570–5575.
[19] Akashi T, Iwata H, Goto T. Preparation of $BaTi_2O_5$ single crystal by a floating zone method. *Mater Trans* 2003, **44**: 802–804.
[20] Akashi T, Iwata H, Goto T. Dielectric property of single crystalline $BaTi_2O_5$ prepared by a floating zone method. *Mater Trans* 2003, **44**: 1644–1646.
[21] Akishige Y, Fukano K, Shigematsu H. New ferroelectric $BaTi_2O_5$. *Jpn J Appl Phys* 2003, **42**: L946.
[22] Zhang J, Yu J, Chao M, *et al.* Textured $BaTi_2O_5$ ceramic

synthesized by laser rapid solidification method and its dielectric properties. *J Mater Sci* 2012, **47**: 1554–1558.
[23] Ashiri R. Obtaining a novel crystalline/amorphous core/shell structure in barium titanate nanocrystals by an innovative one-step approach. *RSC Adv* 2015, **5**: 48281–48289.
[24] Tu R, Goto T. Dielectric properties of poly- and single-crystalline $BaTi_2O_5$. *Mater Trans* 2006, **47**: 2898–2903.
[25] Kimura T, Goto T, Yamane H, *et al*. A ferroelectric barium titanate, $BaTi_2O_5$. *Acta Cryst* 2003, **C59**: i128–i130.
[26] Zhu N, West AR. Formation and stability of ferroelectric $BaTi_2O_5$. *J Am Ceram Soc* 2010, **93**: 295–300.
[27] Li G, Tu R, Goto T. Preparation of polycrystalline $BaTi_2O_5$ by pressureless sintering. *Mater Res Bull* 2009, **44**: 468–471.
[28] Masuno A, Inoue H, Yu J, *et al.* Thermal stability and optical properties of Er^{3+} doped $BaTi_2O_5$ glasses. *Adv Mater Res* 2008, **39–40**: 243–246.
[29] Yu J, Yoda S, Masuno A, *et al.* Structure of glassy and metastable crystalline $BaTi_2O_5$ fabricated using containerless processing. *Ferroelectrics* 2010, **402**: 130–136.
[30] Ahmad J, Alam S, Yu J, *et al.* Effect of Ti on the optical band gap of ferroelectric $BaTi_xO_5$-based bulk glass. *Mod Phys Lett B* 2009, **23**: 2377–2383.
[31] Yu J, Arai Y. Anomalous permittivity during crystallization of $BaTi_2O_5$ glass. *Ferroelectrics* 2006, **333**: 221–226.
[32] Yu J, Arai Y, Masaki T, *et al.* Fabrication of $BaTi_2O_5$ glass-ceramics with unusual dielectric properties during crystallization. *Chem Mater* 2006, **18**: 2169–2173.
[33] Karpukhina N, Hill RG, Law RV. Crystallisation in oxide glasses—A tutorial review. *Chem Soc Rev* 2014, **43**: 2174–2186.
[34] Singh AK, Goel TC, Mendiratta RG, *et al*. Dielectric properties of Mn-substituted Ni–Zn ferrites. *J Appl Phys* 2002, **91**: 6626.
[35] Kumar P, Palei P. Effect of sintering temperature on ferroelectric properties of $0.94(K_{0.5}Na_{0.5})NbO_3$–$0.06LNbO_3$ system. *Ceram Int* 2010, **36**: 1725–1729.